Ocean Modelling 92 (2015) 28–41

Contents lists available at ScienceDirect

Ocean Modelling

journal homepage: www.elsevier.com/locate/ocemod

Parameterization of eddy fluxes based on a mesoscale energy budget

Malte F. Jansen [a,b,c,*], Alistair J. Adcroft [b,c], Robert Hallberg [b,c], Isaac M. Held [b,c]

[a] Department of the Geophysical Sciences, The University of Chicago, Chicago, IL 60637, USA
[b] NOAA Geophysical Fluid Dynamics Laboratory, Princeton, NJ 08540, USA
[c] Program in Atmospheric and Oceanic Sciences, Princeton University, Princeton, NJ 08540, USA

ARTICLE INFO

Article history:
Received 4 February 2015
Revised 15 May 2015
Accepted 27 May 2015
Available online 3 June 2015

Keywords:
Eddy parameterization
Eddy kinetic energy
Eddy diffusivity
Mesoscale
Bottom flow
Rhines scale

ABSTRACT

It has recently been proposed to formulate eddy diffusivities in ocean models based on a mesoscale eddy kinetic energy (EKE) budget. Given an appropriate length scale, the mesoscale EKE can be used to estimate an eddy diffusivity based on mixing length theory. This paper discusses some of the open questions associated with the formulation of an EKE budget and mixing length, and proposes an improved energy budget-based parameterization for the mesoscale eddy diffusivity. A series of numerical simulations is performed, using an idealized flat-bottomed β-plane channel configuration with quadratic bottom drag. The results stress the importance of the mixing length formulation, as well as the formulation for the bottom signature of the mesoscale EKE, which is important in determining the rate of EKE dissipation. In the limit of vanishing planetary vorticity gradient, the mixing length is ultimately controlled by bottom drag, though the frictional arrest scale predicted by barotropic turbulence theory needs to be modified to account for the effects of baroclinicity. Any significant planetary vorticity gradient, β, is shown to suppress mixing, and limit the effective mixing length to the Rhines scale. While the EKE remains moderated by bottom friction, the bottom signature of EKE is shown to decrease as the appropriately non-dimensionalized friction increases, which considerably weakens the impact of changes in the bottom friction compared to barotropic turbulence. For moderate changes in the bottom-friction, eddy fluxes are thus reasonably well approximated by the scaling relation proposed by Held and Larichev (1996), which ignores the effect of bottom friction.

1. Introduction

The ocean circulation is strongly influenced by mesoscale turbulent eddies (e.g., Gill et al., 1974; Johnson and Bryden, 1989; Hallberg and Gnanadesikan, 2006; McWilliams, 2008; Waterman et al., 2011). However, the resolution of most current global ocean models is insufficient to resolve these eddies. Most current IPCC-class climate models use ocean components with typical horizontal resolutions of about one degree or coarser (Flato et al., 2013). Longer-term simulations, as used for paleo-climate applications, require even coarser grids, due to the prohibitive computational costs associated with long-term simulations at high resolution. At resolutions of about one degree or coarser, mesoscale eddies cannot be resolved, and their effects on the transport of tracers and physical properties must be parameterized (e.g., Hallberg and Gnanadesikan, 2006). Even when much higher resolutions are used and eddies are present in the tropics and subtropics, the effects of eddies will still need to be parameterized at higher latitudes and in near-coastal waters (Hallberg, 2013). Mesoscale eddy effects are typically parameterized with a tracer diffusion, which is strongly enhanced in the along-isopycnal direction (Redi, 1982), together with a closure based on Gent and McWilliams (1990) (hereafter: GM). The GM parameterization acts to flatten isopycnals by re-arranging water masses adiabatically. A closure of this form is motivated by the fact that eddies extract available potential energy stored in the mean flow, by rearranging water masses adiabatically (Gent et al., 1995). In an isopycnal layer model (which is naturally adiabatic) the GM parameterization can be described as a diffusion of the interface height between isopycnal layers (Gent et al., 1995; Vallis, 2006; Hallberg, 2013). A major question that remains is what sets the eddy tracer and interface height diffusivities. It is clear that both coefficients should vary in space and depend on properties of the resolved flow itself. Some dependence of the eddy diffusivity on the resolved flow is now commonly included in numerical ocean models (e.g., Farneti and Gent, 2011). However, exactly how this dependence should look remains unclear - yet it is of primary importance for the response of eddy transports to changes in the external forcing.

It has recently been proposed to formulate the eddy diffusivity based on a mesoscale eddy kinetic energy (EKE) budget (Cessi, 2008; Eden and Greatbatch, 2008; Marshall and Adcroft, 2010). Both the

* Corresponding author. Tel.: +1 617 230 0262.
E-mail address: mfj@uchicago.edu (M.F. Jansen).

http://dx.doi.org/10.1016/j.ocemod.2015.05.007
1463-5003/

tracer and interface height eddy diffusivities are expected to scale with a typical eddy velocity times a mixing length. The eddy velocity can be inferred from the EKE, leaving the mixing length scale to be specified. A generally applicable scaling relation for the mixing length has not yet been derived. However, even assuming a constant mixing length, an EKE budget based parameterization may be expected to be superior to the assumption of a constant eddy diffusivity, as it takes into account the dependence of the eddy velocity on the mean state.

The goal of this paper is to build upon some of the arguments proposed by Cessi (2008) , Eden and Greatbatch (2008) and Marshall and Adcroft (2010). We will analyze a series of idealized numerical simulations, test some of the assumptions made in these previous studies, and discuss their implications for the estimated eddy diffusivity. Based on these considerations, we will propose an improved parameterization for the mesoscale eddy tracer diffusivity and GM transfer coefficient.

One focus here will be on the role of frictional dissipation. The EKE level in a statistical equilibrium is controlled by a balance between the net transfer of energy from the large-scale mean flow to EKE (by instabilities of the mean flow) and the dissipation of EKE. It has therefore been argued repeatedly that frictional dissipation must be important in controlling the level of EKE and with it the eddy diffusivity (e.g., Arbic and Flierl, 2004; Thompson and Young, 2007; Arbic and Scott, 2008; Cessi, 2008). However, none of the traditional parameterizations for the mesoscale eddy diffusivity (e.g., Green, 1970; Stone, 1972; Held and Larichev, 1996; Visbeck et al., 1997) includes any explicit dependence on parameters characterizing frictional dissipation. Of the EKE budget based arguments cited above, only Cessi (2008) and Marshall and Adcroft (2010) explicitly consider the role of frictional dissipation. In both cases frictional dissipation is described by a simple linear loss term in the EKE budget, seemingly consistent with the linear bottom drag assumed in the numerical simulations considered in these studies.

In addition to the role of frictional dissipation on the eddy energy budget, we will also make a new attempt at characterizing what sets the eddy mixing length. In the limit of vanishing planetary vorticity gradient and topography, the mixing length is ultimately limited by bottom friction. However, the frictional arrest scale predicted by barotropic turbulence theory (Grianik et al., 2004; Held, 1999) needs to be modified to include effects associated with baroclinicity. Moreover, any significant planetary vorticity gradient, β, is shown to suppress mixing, and limit the effective mixing length to the Rhines scale.

This paper focusses on some of the theoretical challenges in the formulation of the EKE budget and mixing length. A variant of the EKE budget equation is introduced in Section 2. In Section 3, we show results from a series of idealized numerical simulations, with the discussion focussing primarily on the mixing length, as well as the vertical structure of EKE - which controls the dissipation rate of EKE via bottom friction. In Section 4, we then use the results for the mixing length and vertical structure of EKE to derive a scaling relation for the eddy diffusivity, assuming a spatially and temporally local balance of EKE generation and dissipation (similar to Cessi, 2008). In Section 5, we discuss some outstanding questions and directions for future work, and we conclude with a summary of the main results in Section 6.

2. The EKE budget

Eden and Greatbatch (2008) formulate a predictive equation for the three-dimensional field of mesoscale eddy kinetic energy, for use in a numerical model which does not resolve the mesoscale flow. Such a local budget leaves some arbitrariness as to the exact formulation of large-scale to mesoscale energy transfer terms, with different formulations differing by flux terms, which vanish in a global integral, but may be large locally. Moreover, using any formulation, flux terms do arise and need to be parameterized. This provides a challenge in particular for the computation of the vertical structure of mesoscale EKE, which typically organizes mostly into the barotropic and lowest baroclinic modes (Wunsch, 1997). For simplicity, we here formulate a budget equation only for the total vertically integrated mesoscale EKE (as also done by Cessi, 2008), thus circumventing the need for an explicit parameterization of vertical EKE fluxes.

If we assume that the effect of mesoscale eddies on the large scale flow is represented by the GM parameterization and a viscous stress term, we can write the mesoscale EKE budget equation as

$$\partial_t E = \dot{E}_{GM} - \dot{E}_{fric} - \nabla \cdot \mathbf{T}. \tag{1}$$

$\dot{E}_{GM}$ is the energy loss of the large-scale flow associated with the GM parameterization - which parameterizes the conversion of large-scale available potential energy into mesoscale EKE by baroclinic instability. $\dot{E}_{fric}$ represents frictional dissipation of mesoscale EKE, and $\mathbf{T}$ denotes the horizontal transport of mesoscale EKE.

The simulations discussed in this paper employ an isopycnal layer model, in which the effect of the GM parameterization is obtained by a diffusion of the layer interface height, and thus

$$\dot{E}_{GM} = \frac{1}{H}\sum_i g_i' K_\eta |\nabla \overline{\eta}_i|^2 \tag{2}$$

where H is the total depth, g_i' is the reduced gravity at the ith layer interface, $\overline{\eta}_i$ is the interface height displacement of the large-scale "resolved" flow, and K_η is the interface height diffusivity, which is analog to the GM coefficient in a $z-$coordinate model (Gent et al., 1995; Vallis, 2006; Hallberg, 2013). The sum is here taken over all layer interfaces. As mentioned above, there is some freedom as to how exactly this term is formulated, with the difference between formulations amounting to a flux term, which vanishes upon global integration but not locally. The formulation in Eq. (2) has the desirable property that it is locally positive definite.

We don't include a direct transfer of kinetic energy between the large-scale resolved flow and the mesoscale eddies. A direct transfer from large-scale KE to mesoscale EKE represents the source of EKE in barotropic instability (e.g. Marshall and Adcroft, 2010), which, however, is not expected to be important in the simulations discussed below. In general, the sign of the net kinetic energy transfer between the large-scale flow and mesoscale eddies remains unclear. Jansen and Held (2014) propose to include a "backscatter" of KE from subgrid scales to the resolved flow in eddy permitting models, to represent the up-scale transfer of EKE in geostrophic turbulence. Even at coarser, non-eddying, resolution such a backscatter term (which can drive jets and Taylor caps) may be of at least similar magnitude to the potential source of mesoscale EKE associated with barotropic instability. For simplicity neither barotropic instability nor energy backscatter are included in the EKE budgets discussed here.

$\dot{E}_{fric}$ is the frictional dissipation of EKE. Unlike three-dimensional isotropic turbulence, geostrophic turbulence does generally not exhibit a direct kinetic energy cascade towards the micro-scale, where energy can be dissipated effectively by the molecular viscosity. This lack of a direct EKE cascade opens up the question of how mesoscale EKE is dissipated in the ocean. While the exact pathways of mesoscale EKE to dissipation remain unknown and heavily debated (e.g. Wunsch and Ferrari, 2004; Ferrari and Wunsch, 2009), there is both observational and numerical evidence for strongly enhanced dissipation near the bottom boundary, where rough topography generates energy transfers into internal waves and boundary layer turbulence (e.g. Ledwell et al., 2000; Nikurashin et al., 2013). In the numerical simulations discussed in this study frictional dissipation near the bottom boundary is parameterized using a quadratic bottom drag. A quadratic drag law follows directly from dimensional considerations, and is widely used in numerical ocean models (Egbert et al., 2004; Gill, 1982; Willebrand et al., 2001). Consistent with our numerical model we formulate the frictional dissipation of

mesoscale EKE as

$$\dot{E}_{fric} = \frac{C_D}{H}|U_b|2E_b. \tag{3}$$

Here $|U_b| = [U_0^2 + |\overline{\mathbf{v}}(z=-H)|^2 + 2E_b]^{1/2}$ is the total velocity near the bottom. $|\overline{\mathbf{v}}(z=-H)|^2$ is the large-scale (resolved) flow in the bottom layer, and U_0 is an unresolved background velocity, representing e.g. tidal motions, which effectively leads to an additional linear drag component. Notice, that it is only the EKE near the bottom, E_b, which enters the dissipation via bottom friction. To obtain a closed budget for the mesoscale EKE, we thus need to know the ratio of the EKE near the bottom to the total EKE. This parameter will be discussed in more detail in Section 3.5.

While appropriate for the numerical simulations discussed in this study, it remains an open question whether Eq. (3) adequately captures the bulk of the mesoscale EKE dissipation in the real ocean. A better understanding of the pathways to dissipation of mesoscale EKE in the real ocean thus remains an important topic of future research (see also Section 5).

T denotes the horizontal transport of EKE. Eden and Greatbatch (2008) and Marshall and Adcroft (2010) parameterize this term by a diffusion of EKE and advection by the resolved large-scale flow. In practice flow-relative eddy propagation is arguably at least as important as mean flow advection, with the former dominating the net eddy propagation over most of the ocean (e.g., Chelton et al., 2007; Klocker and Abernathey, 2014; Klocker and Marshall, 2014).[1] Cessi (2008) ignores the transport of EKE, assuming a local balance between generation and dissipation of EKE. A similar approach will be followed here. The assumption of a local mesoscale EKE balance is expected to be adequate for most of our simulations, which use a zonally symmetric channel model. However, an accurate parameterization of EKE transports will likely be of greater importance in a more realistic ocean configuration, and thus provides an important topic for future work.

2.1. The tracer diffusivity and GM coefficient

Once an EKE budget is formulated, it can be used to infer an eddy diffusivity. Here, we are primarily interested in the interface height diffusivity, which appears in the energy budget equation (1). The passive tracer and potential vorticity (PV) diffusivities are expected to scale largely similarly to the interface height diffusivity in a bulk sense, though their vertical structures may differ substantially (e.g., Abernathey et al., 2013). In the two-layer simulations discussed below, the PV diffusivities in both layers can be inferred directly from the interface height diffusivity, as long as the flow is well approximated by planetary geostrophic scaling (Vallis, 1988). In the limit that the contribution of β to the PV gradient is small, all diffusivities are identical.

Mixing length theory (Plumb, 1979; Prandtl, 1925) suggests that the eddy diffusivity scales as the product of a characteristic eddy velocity times a mixing length, L_{mix}:

$$K \sim \sqrt{E} \times L_{mix}. \tag{4}$$

Cessi (2008), Eden and Greatbatch (2008), and Marshall and Adcroft (2010) all use the formulation in Eq. (4), but with differing assumptions for the mixing length, L_{mix}. In the following section we will analyze a range of numerical simulations to test the scaling relation in Eq. (4) and determine what controls the mixing length.

Cessi (2008) argues that the characteristic eddy velocity should be based on the barotropic mode EKE only, since the geostrophic flow associated with a given baroclinic mode cannot advect baroclinicity associated with that same mode. This argument is expected to hold well if the flow is dominated by the barotropic and first baroclinic mode only, which is likely to be true over most of the ocean (Wunsch, 1997). The argument is also expected to hold in the two-layer model simulations discussed below, which by construction support only one baroclinic mode.

3. Numerical simulations

3.1. Model description

We performed a series of numerical simulations using a flat-bottomed, periodic channel configuration of MOM6, with two adiabatic vertical layers, similar to the setup discussed by Hallberg (2013). The domain is 1600 km wide in the meridional direction, 1200 km long in the zonal direction, and 2000 m deep. The zonal mean interface height (in the following loosely referred to as "pycnocline depth") is restored to a hyperbolic tangent profile on a relatively fast time-scale (10d), but with no damping of anomalies relative to the zonal mean. Like a zonally-symmetric wind-stress, the forcing thus does not directly impact the eddy energy budget. The baroclinic zone is here somewhat wider than in Hallberg (2013), with a hyperbolic tangent profile with a characteristic width of 800 km. The pycnocline depth varies across the baroclinic zone from about 800 m in the south to about 200 m in the north. The equilibrium solution for the restoring is shown in Fig. 1. EKE is dissipated primarily by bottom drag, which is described via a quadratic drag law, as discussed in Section 2. A weak background velocity $U_0 = 1\,\mathrm{cm\ s^{-1}}$ is included in the formulation of the bottom drag, but has relatively little impact in the more energetic region near the center of the jet. Enstrophy is dissipated near the grid-scale using a biharmonic viscosity, with a viscosity coefficient following Smagorinsky (1963) (see Griffies and Halberg, 2000, for the biharmonic formulation applied here).

A series of simulations is analyzed, with differing buoyancy contrasts across the two layers: $\Delta\rho/\rho_0 = (0.75, \mathbf{1.5}, 3.0) \times 10^{-3}$, differing Coriolis parameters: $f_0 = (0.56, \mathbf{1.1}, 2.2) \times 10^{-4}\ \mathrm{s^{-1}}$, and differing planetary vorticity gradients: $\beta = (0, 0.75, \mathbf{1.5}, 3) \times 10^{-11}\ \mathrm{m^{-1}\ s^{-1}}$. The simulations use a β-plane approximation, with f_0 here referring to the Coriolis parameter in the middle of the domain. The planetary vorticity gradient, $\beta = \partial_y f$ is constant over the domain. Each parameter is varied separately with the other parameters fixed at their reference value (marked above in bold face), which yields 8 different parameter sets. For all resulting parameter sets, the bottom drag coefficient is varied between 8 values:

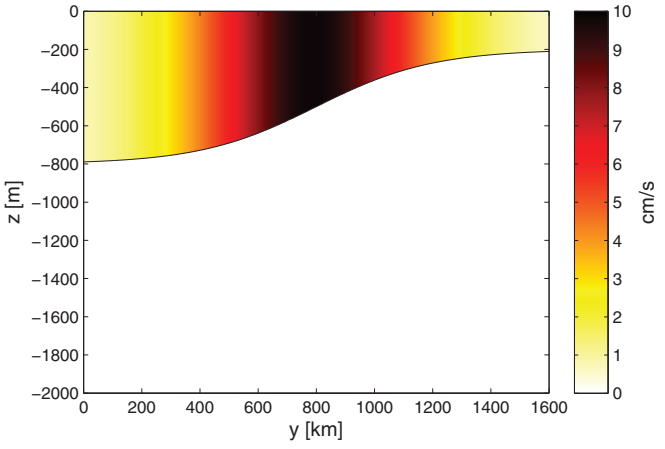

Fig. 1. Interface height (grey line) and associated geostrophic velocity (shading) for the equilibrium solution of the restoring forcing. The bottom layer is motionless due to the lack of a momentum forcing and presence of bottom drag.

[1] Some of this work focuses on the observed or inferred eddy *phase* speeds, while EKE is expected to propagate with the group velocity. However, it also appears that the dispersion relation typically shows only weakly dispersive behavior, suggesting that phase and group-propagation are likely to be roughly similar (e.g. Early et al., 2011, and references therein).

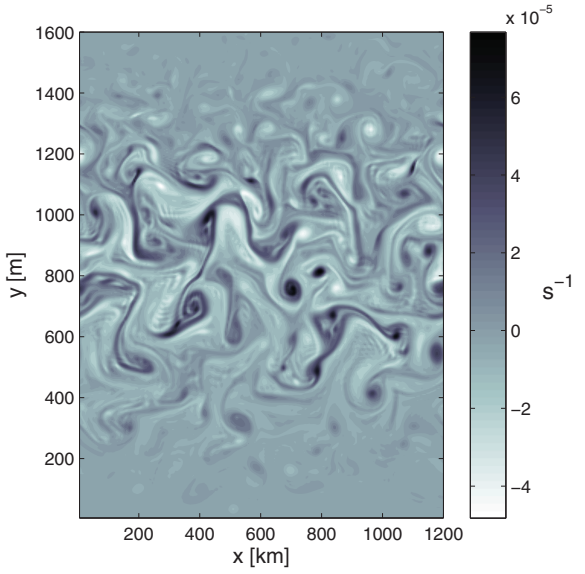

Fig. 2. Snapshot of upper-layer relative vorticity for the reference simulation with $C_d = 0.01$.

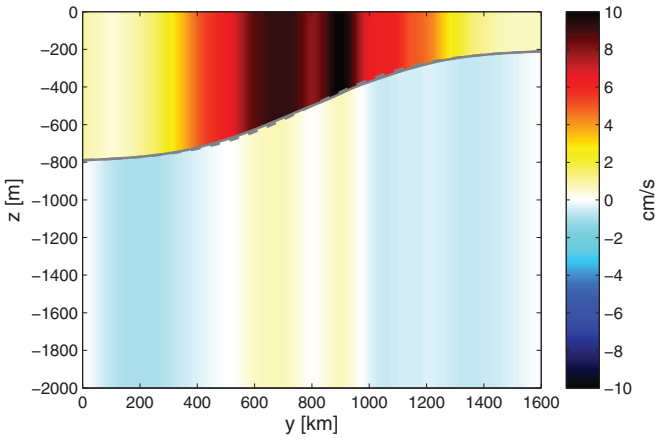

Fig. 3. Time and zonal mean interface height (solid gray line) and zonal velocity (shading) for the reference simulation with $C_d = 0.01$. The dashed grey line (largely indistinguishable from the solid gray line) shows the interface height for the equilibrium solution of the restoring forcing.

$C_d = (0.625, 1.25, 2.5, 5, 10, 20, 40, 80) \times 10^{-3}$, which yields a total of $8 \times 8 = 64$ simulations. The bottom drag coefficient is typically assumed to be constant in ocean models, which might make it seem irrelevant to consider a range of simulations with varying bottom drag. The reasoning to consider a wide range of bottom drags here is at least two-fold. First, there is a theoretical interest in exploring the role of frictional dissipation in controlling the eddy statistics. Moreover, we will argue below that the relevant non-dimensional parameter characterizing the role of frictional drag, is the ratio of a frictional length scale to the deformation radius, which may vary considerably even if the drag coefficient remains constant. Eventually, the drag coefficient may indeed vary significantly in the real ocean, depending on the small-scale topographic roughness (e.g. Özgökmen and Fischer, 2008).

The total range of deformation radii over the domain and parameter-range used here extends from 8.1 km at the northern end of the domain in the simulations with $f_0 = 2 \times 10^{-4}$ s^{-1} to 53 km at the southern end of the domain and for the simulations with $f_0 = 0.5 \times 10^{-4}$ s^{-1}. Near the center of the baroclinic jet, the smallest deformation radius is about 12 km (again for the simulations with $f_0 = 2 \times 10^{-4}$ s^{-1}). Using a similar setup, Hallberg (2013) showed that a resolution of one to two grid-points per deformation radius is sufficient to obtain adequately resolved eddy fluxes, with the exact value dependent on the supercriticality of the background flow. Based on these results, we choose a grid-spacing of 5 km, which should be adequately eddy-resolving over the entire parameter range. All simulations are spun-up to a statistical equilibrium for 10 years, and statistics are computed for 10 years following this initial spin-up period.

Notice that our model setup is highly idealized, and lacks several ingredients that may be of importance in the real ocean, such as continental boundaries, bottom topography, or higher vertical modes (which would require more vertical levels). This and the following section will focus on understanding and parameterizing the turbulent flow properties arising in this idealized numerical model. The limitations of the model for the interpretation of processes in the real ocean will be discussed in Section 5.

3.2. General results

Fig. 2 shows a snapshot of relative vorticity in the upper layer for a simulation with the reference case parameters and $C_d = 1 \times 10^{-2}$. We see vigorous eddy activity in the baroclinically forced region between about $y = 400$ km and $y = 1200$ km. Fig. 3 shows the zonal mean flow associated with this simulation. Due to the fast restoring of the zonal mean interface height, the large-scale slope of the interface changes little relative to the restoring profile, despite the obvious vigorous eddy activity. Since the flow is largely geostrophically balanced, this implies relatively small deviations of the large-scale baroclinic mean flow from the equilibrium state of the restoring (compare to Fig. 1). However, two localized eastward jets are spun up near the domain center, which extend into the lower layer. The eastward jets in the lower layer are accompanied by broader westward flows further north and south. The lower layer flow here is driven entirely by eddy momentum fluxes, since the frictional drag acting on the deep-ocean flow is balanced only by the vertically integrated eddy momentum flux convergence. Lower layer jets thus cannot be generated if eddy effects are parameterized solely by a GM parameterization, or interface height diffusion, which does not generate a net momentum flux. The snapshot in Fig. 2 suggests that the jets here are relatively weak as compared to the eddies, and thus become apparent only in time- and zonal averages.

3.3. The bulk eddy diffusivity

In this paper we are most interested in the eddy-driven mass transport, which can be related to the mean baroclinicity by an eddy interface height diffusivity, and which typically represents the major source of EKE (see Eq. (2)). Since the domain and forcing are zonally symmetric, it is natural to define eddies as deviations from the zonal average. Due to mass continuity, the long-term mean eddy driven mass transport in the upper and lower layer are approximately equal and opposite, and we can compute an eddy driven overturning circulation as

$$\Psi^\dagger \equiv \langle \overline{v_1' h_1'} \rangle, \tag{5}$$

where v_1 and h_1 represent the upper layer meridional velocity and layer thickness, respectively. The overbar denotes a zonal average, with primes denoting deviations from the zonal mean, and $\langle\rangle$ denotes a time average, here taken over the last ten years of each simulation. The resulting eddy driven overturning transports are shown in Fig. 4, for three example simulations, with the reference parameter values for f_0, β, and $\Delta\rho/\rho_0$, but three different values for the bottom drag coefficient: the lowest, highest and one intermediate value. As expected, the eddy driven overturning circulation is overall largest where the baroclinic forcing is strongest and decays towards the northern and southern ends of the domain. The peak overturning

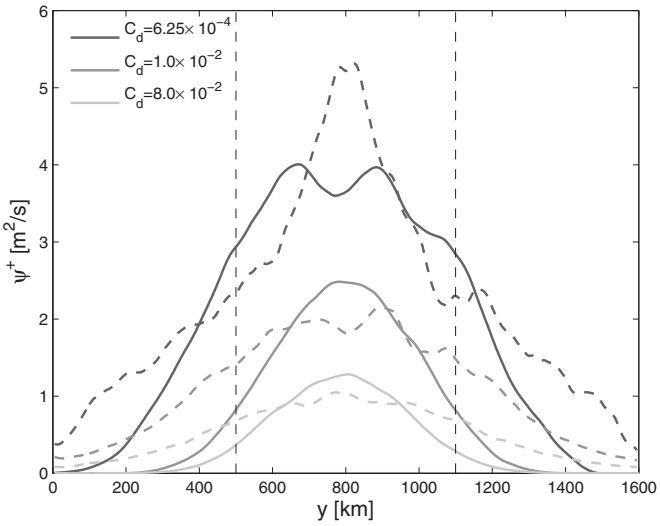

Fig. 4. Solid: eddy-driven overturning mass transport for three different values of the drag coefficient (see legend). Dashed: overturning mass transport inferred by using a diffusive closure for the thickness flux with a constant eddy diffusivity computed separately for each case as defined in Eq. (6) . The thin vertical dashed lines indicate the region that is used to compute averaged quantities.

circulation varies between about 1 $m^2\ s^{-1}$ for the simulation with the strongest frictional drag, to about 4 $m^2\ s^{-1}$ in the simulation with the weakest drag. If we were to extrapolate this to a 20000 km circumpolar channel, we would obtain an overturning transport of about 20–80 Sv, which is on the same order as the eddy driven overturning transport in the antarctic circumpolar current (ACC), with the lower end likely being more realistic (e.g. Mazloff et al., 2013).

While Fig. 2 through 4 show obvious meridional variations in the eddy and mean flow statistics, the focus of this paper is on the bulk parametric dependence of the eddy diffusivity. For this purpose we will compute averaged quantities for each simulation, with averages taken over the more strongly baroclinic region in the center of the domain, between $y = 500$ km and $y = 1100$ km. Specifically, a bulk horizontal eddy interface-height diffusivity is defined as

$$[K] \equiv \frac{[\Psi^\dagger]}{[\langle \partial_y \overline{\eta} \rangle]}, \tag{6}$$

where $\partial_y \eta$ is the slope of the layer interface and [ ] denotes the meridional average. Notice that $\Psi^\dagger = \overline{v_1' h_1'} \approx \overline{v_1' \eta'} \approx \overline{v_t' \eta'}$, where v_t is the barotropic velocity. In the second step we ignored the (very small) contributions to the layer thickness associated with the free surface, while in the last step we made the geostrophic approximation, which implies that $\overline{(v_1 - v_2)' \eta'} \propto -\overline{\partial_x \eta' \eta'} = 0$. The quantity defined by Eq. (6) can thus be interpreted as an eddy interface height diffusivity, which is governed by the barotropic flow. The definition in (6) is also equivalent to the GM coefficient in a z-coordinate model (e.g., Gent et al., 1995; Vallis, 2006). The time- and meridional-averages in Eq. (6), are taken separately in the numerator and denominator to ensure that the bulk eddy diffusivity remains well defined if the interface height slope is weak at certain times and locations. Fig. 4 shows estimates of the time-mean eddy driven overturning circulation obtained by multiplying the thus defined eddy diffusivity by the zonal mean interface height slope. The bulk eddy diffusivity successfully captures the bulk eddy transport over the region used to compute the average. However, Fig. 4 also shows that a globally constant eddy diffusivity would yield a poor representation of the local eddy transport in some regions.

The bulk eddy diffusivity obtained for all simulations is shown in Fig. 5a, as a function of the drag parameter. The eddy diffusivity varies widely with both the frictional drag as well as other parameter changes, ranging from about 400 $m^2\ s^{-1}$ to about 50,000 $m^2\ s^{-1}$. The reference setup at realistic intermediate drag values has diffusivities around 4000 $m^2\ s^{-1}$, which is significantly larger than values typically found over most the ocean (e.g. Abernathey and Marshall, 2013). Relatively large eddy diffusivities are expected for our reference case setup, because the baroclinicity is characteristic of that found in the more energetic regions of the Southern Ocean (which served as a rough motivation for the setup), while the deformation radius is significantly larger than in the Southern Ocean. This is not likely to limit the interpretability of the results in the context of the real ocean, since the dynamical properties of the flow depend only on the non-dimensional parameters (which will be discussed

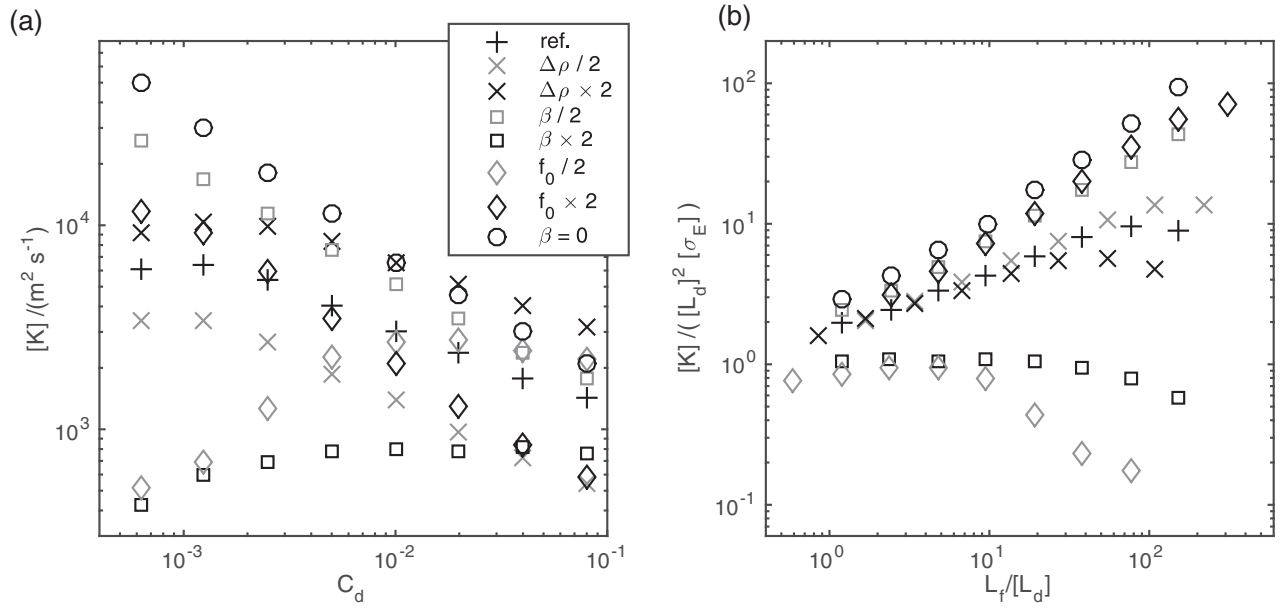

Fig. 5. (a) Eddy diffusivity against the bottom drag coefficient for all simulations performed for this study. (b) Eddy diffusivity non-dimensionalized by $[L_d]$ and $[\sigma_E]$ against the non-dimensionalized frictional length scale $L_f/[L_d]$. In both figures, pluses denote the simulations with the reference parameter set, crosses denote the simulations with doubled (black) and halved (gray) layer density contrast $\Delta\rho$, squares denote the simulations with doubled (black) and halved (gray) planetary vorticity gradient β, diamonds denote the simulations with doubled (black) and halved (gray) Coriolis parameter f_0, and circles denote the simulations with $\beta = 0$.

Table 1
Overview of derived bulk quantities defined in this paper (see text for details). Dimensions are given in terms of length (L) and time (T). All non-dimensionalized quantities discussed in this paper are normalized using the deformation radius and Eady growth rate (marked in bold).

Symbol	Description	Definition	Dimensions
$[\boldsymbol{L_d}]$	Deformation radius	$\left[\left\langle \frac{\sqrt{g'\overline{h_e}}}{f} \right\rangle\right]$	L
$[\boldsymbol{\sigma_E}]$	Eady growth rate	$\sqrt{g'/H}[\langle \partial_y \overline{\eta} \rangle]$	T^{-1}
$[K]$	Eddy (interface-height) diffusivity	$\frac{[\overline{\psi' v'}]}{[\langle \partial_y \overline{\eta} \rangle]}$	L^2T^{-1}
$[E]$	Eddy kinetic energy (EKE)	$\frac{[\langle \overline{h_1(u_1'^2+v_1'^2)+h_2(u_2'^2+v_2'^2)} \rangle]}{2H}$	L^2T^{-2}
$[E_b]$	Bottom EKE	$\frac{[\langle \overline{u_2'^2+v_2'^2} \rangle]}{2}$	L^2T^{-2}
$[E_t]$	Barotropic EKE	$\frac{[\langle \overline{(h_1u_1+h_2u_2)^2+(h_1v_1+h_2v_2)^2} \rangle]}{2H^2}$	L^2T^{-2}
γ	Bottom to barotropic EKE ratio	$[E_b]/[E_t]$	None
L_f	Frictional scale	H/C_d	L
$[L_R]$	Rhines scale	$[E_t]^{1/4}\beta^{-1/2}$	L
L_{BC}	Width of baroclinic zone	800 km	L
$[L_{LH}]$	Effective mixing length implied by Larichev and Held (1995) scaling	$[E_t]^{1/2}[\sigma]^{-1}$	L
$[L_{arr}]$	Effective frictional arrest scale	$\gamma^{-3/2}L_f$	L

below). The lack of topography in our simulations likely causes another bias towards larger eddy diffusivities, as compared to the real ocean. We will return to this issue in the discussion.

For most of the parameter sets considered here, the eddy diffusivity increases as the frictional drag is reduced, which might be expected considering the reduced dissipation of eddy energy. However, for the simulations with doubled planetary vorticity gradient (black squares) and halved Coriolis parameter (gray diamonds), the eddy diffusivity instead decreases for low frictional drag values. At the very weakest drag values, a slight decrease in the eddy diffusivity is also found in some of the other simulations.

To understand the variability of the eddy diffusivity observed in 5a, it is helpful to consider the most relevant non-dimensional parameters. Following homogeneous, quasi-geostrophic scaling, we may expect the four most relevant dimensional parameters to be given by the deformation radius, L_d, an Eady growth rate, σ_{Eady}, the planetary vorticity gradient, β, and a frictional length scale $L_f \sim H/C_d$. L_f may be thought of as the scale at which the frictional decay time-scale for a barotropic perturbation, $\tau_f \sim L_f U^{-1}$, equals the eddy overturning time-sale, $\tau_{eddy} \sim LU^{-1}$. In barotropic turbulence, L_f represents the halting scale of the inverse energy cascade Grianik et al. (2004); Held (1999). Normalizing length scales by L_d and time-scales by σ_{Eady}, we are left with two non-dimensional parameters: the non-dimensionalized frictional length scale, L_f/L_d, and the non-dimensionalized planetary vorticity gradient, $\beta^* \equiv \beta L_d/\sigma_{Eady}$, which is inversely proportional to the super-criticality of the flow to baroclinic instability.[2] Notice that the Eady growth rate is proportional to $\Delta U/L_d$, where ΔU denotes the shear velocity between the two vertical layers. The normalization used here is thus analogous to one using the deformation radius and baroclinic shear.

For the present model, a bulk deformation radius can be defined as

$$[L_d] \equiv \left[\left\langle \frac{\sqrt{g'\overline{h_e}}}{f} \right\rangle\right], \tag{7}$$

with the averages defined as before. $g' \equiv g\Delta\rho/\rho$ is the reduced gravity for the layer interface, and $h_e = h_1h_2/(h_1+h_2)$ is the equivalent depth scale for the baroclinic mode. A bulk Eady growth rate can be defined as

$$[\sigma_E] = \sqrt{g'/H}[\langle \partial_y \overline{\eta} \rangle], \tag{8}$$

where H is the total depth.[3] A summary of all the derived quantities defined in this paper is given in Table 1.

Fig. 5b shows the eddy diffusivity normalized by $L_d^2\sigma_E$, as a function of L_f/L_d. We first note that the normalized eddy diffusivity varies at least as widely over the considered set of simulations as the dimensional eddy diffusivity, suggesting that the deformation radius and Eady growth rate alone do not explain much of the variability. The dependence of the normalized eddy diffusivity on the normalized drag is similar to what is observed without the normalization: the diffusivity mostly increases with reduced drag (larger L_f/L_d), though the smallest diffusivities are found in the weak-drag limit of the simulations with doubled planetary vorticity gradient (black squares) and halved Coriolis parameter (grey diamonds).

The simulations considered here can be grouped into four different sets based on their non-dimensional planetary vorticity gradient, or super-criticality. Due to the fast zonal mean restoring, the layer depths and slope of the layer interface change little over the considered range of simulations, so that to a reasonably good approximation $\beta* = \beta L_d/\sigma_{Eady} \propto \beta/f$. Changes in the density contrast thus have little impact on β^*. A doubling of β or halving of f both lead to a doubling of β^*, while a doubling of f or halving of β both lead to a halving of β^*. β^* is zero for the simulations with $\beta = 0$. Fig. 5b shows that simulations with large β^* (weak super-criticality) generally have weaker eddy diffusivities, while simulations with small β^* (strong super-criticality) have larger eddy diffusivities, for similar values of the normalized drag. Most of the variability in the eddy diffusivity appears to be explained by the two non-dimensional parameters – particularly for strong and moderate drag. However, at weak drag there remain significant discrepancies between the eddy diffusivities of simulations with almost identical non-dimensional parameters. These discrepancies are likely primarily due to spatial inhomogeneities – we will return to this issue below.

The dependence of the normalized eddy diffusivity on the super-criticality is in qualitative agreement with many previous studies (e.g. Held and Larichev, 1996; Thompson and Young, 2007; Jansen and Ferrari, 2013). The dependence of the normalized eddy diffusivity

[2] In the two layer model, the super-criticality of the system to baroclinic instability generally depends on $\beta L_d/\sigma_{Eady}$, as well as the ratio between the upper and the lower layer depth, which is held constant here (e.g., Nakamura and Wang, 2013). As argued by Flierl (1978), the two mode interpretation of the two-layer model suggests that the layer depth ratio may be interpreted as the surface intensification of the stratification. The role of this parameter has been discussed by Arbic and Flierl (2004).

[3] There is some arbitrariness as to what depth scale to use to estimate the Eady growth rate, which has originally been defined only for a fluid with constant stratification - which is roughly analogous to a two-layer setup with equal layer depth (Flierl, 1978). The definition here was chosen such that the energy extraction associated with an interface height diffusion generally scales with the interface height diffusivity times σ_E^2 (see Section 4). Since all layer depths are held constant in the simulations discussed here, alternative definitions would only impact constant factors.

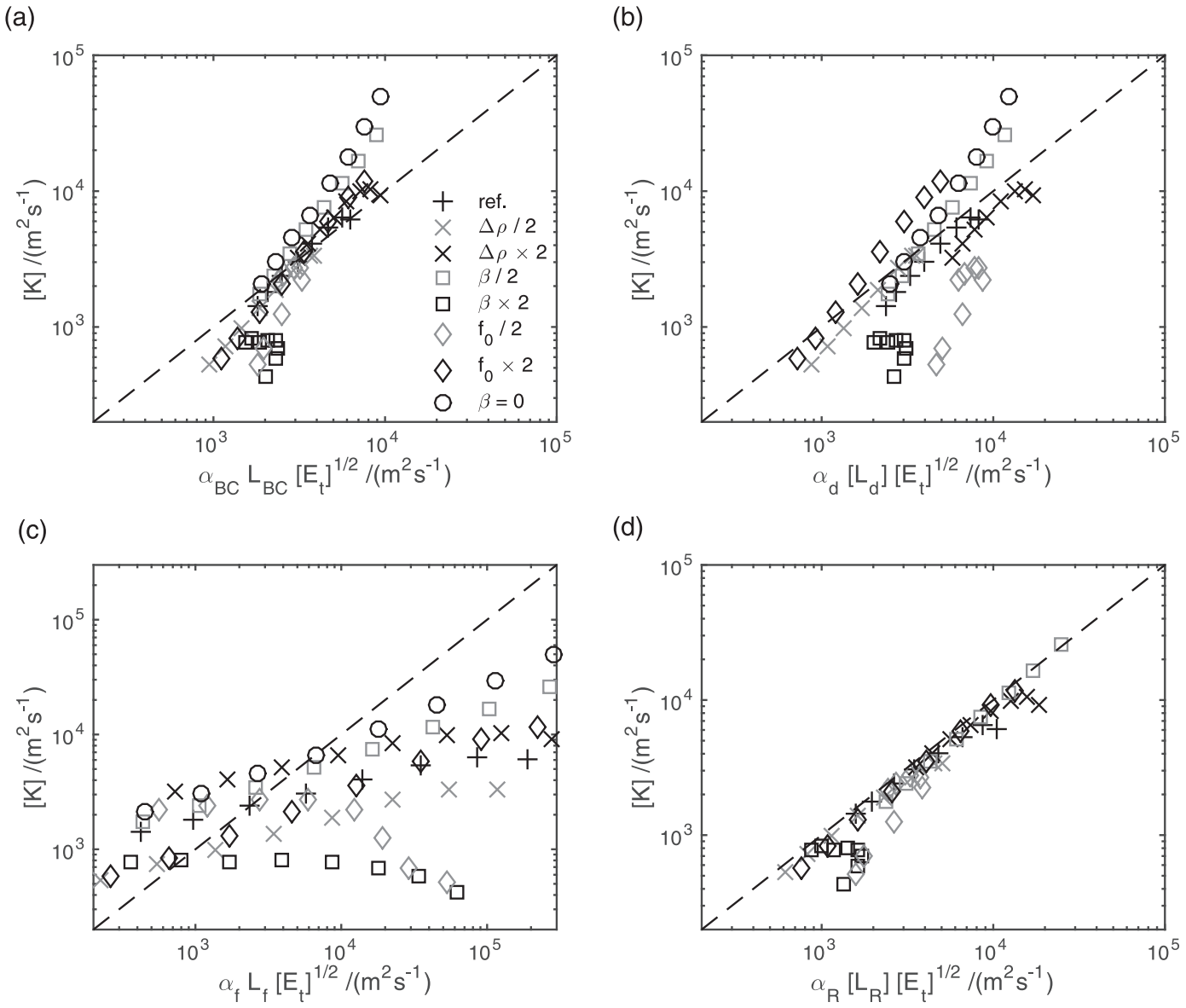

Fig. 6. Bulk eddy diffusivity against estimates based on a mixing length argument: $K = E_t^{1/2} L_{mix}$, with E_t the diagnosed barotropic EKE, and various choices for the mixing length: (a) $L_{mix} = \alpha_{BC} L_{BC}$ = const, where $\alpha_{BC} = 0.04$ (b) $L_{mix} = \alpha_d [L_d]$, with $\alpha_d = 2.0$, (c) $L_{mix} = \alpha_f L_f$, with $\alpha_f = 0.3$, and (d) $L_{mix} = \alpha_R [L_R]$, with $\alpha_R = 0.45$. The constant coefficients, α_x, were chosen empirically to match the data. The markers used for the different sets of simulations are as in Fig. 5. Notice that panel (c) has an increased axis-range to include the very large diffusivity estimates.

on the frictional drag qualitatively resembles the results reported by Thompson and Young (2007), who find that the eddy diffusivity decreases with increasing drag for moderately and highly supercritical mean states, while the eddy diffusivity increases with drag for weakly supercritical mean states. This qualitative similarity comes despite of the use of a linear friction in Thompson and Young (2007), where the non-dimensional drag coefficient is computed as the ratio of the drag rate to the Eady growth rate.

3.4. The mixing length

Eq. (4) formulates an eddy diffusivity in terms of the EKE and a mixing length. To isolate the question of what sets the mixing length, we compute estimates of the eddy diffusivity based on the diagnosed EKE, and various formulations for the mixing length. Since the eddy interface height diffusivity is expected to be controlled by the barotropic flow, estimates are computed as

$$K = [E_t]^{1/2} L_{mix}, \tag{9}$$

where E_t denotes the barotropic EKE, and different quantities will be chosen for the mixing length. Using the total EKE instead of the barotropic component yields qualitatively similar results, but the best fit to the observed eddy diffusivity shows somewhat more spread.

Fig. 6 tests Eq. (9) using four different formulations for the eddy mixing length: 1) the total width of the baroclinic region, L_{BC} (Green, 1970; Visbeck et al., 1997), 2) the baroclinic deformation radius, L_d (Stone, 1972), 3) the frictional halting scale, L_f (Grianik et al., 2004; Held, 1999), and 4) the Rhines scale, L_R, (Held and Larichev, 1996; Rhines, 1979). Due to the fast zonal-mean interface height restoring, L_{BC} is here well approximated by a constant: $L_{BC} \equiv 800$ km. A constant mixing length is also commonly used in climate model implementations of the Visbeck et al. (1997) parameterization (e.g., Farneti and Gent, 2011). The Rhines scale is computed based on the diagnosed barotropic EKE: $[L_R] \equiv [E_t]^{1/4} \beta^{-1/2}$.

Fig. 6 a, suggests that the barotropic EKE by itself is a useful predictor of the eddy diffusivity, but the combination with a constant mixing length appears to underestimate the dependence of the eddy

diffusivity on the EKE level. Replacing the mixing length with the deformation radius worsens the fit, suggesting that L_d is not a useful predictor of the mixing length (Fig. 6b). The frictional scale, L_f, appears to over-estimate the sensitivity of the eddy diffusivity to the bottom drag (Fig. 6c).

A very good fit is obtained for most simulations if the mixing length is chosen as the Rhines scale (Fig. 6d). Some limitations remain in the limit of very low friction and in the weakly super-critical simulations with small f_0 or large β, which show lower eddy diffusivities than predicted. In these limits the eddies tend to spin up strong barotropic jets, with large associated horizontal shears. It appears that these shear flows suppress baroclinic instability and eddy mixing as discussed by James and Gray (1986), who dubbed this effect the "barotropic governor". The results of Zurita-Gotor (2007) suggest that this effect might be captured by including the barotropic vorticity gradient of the zonal mean flow in the definition of a generalized β. A predictive theory which incorporates this generalization would require a theory for the vorticity of the barotropic jets, which is beyond the scope of this study. More generally the Rhines scale here provides an upper bound on the mixing length. The Rhines scale, however, provides no bound for the mixing length in the limit of $\beta \to 0$, where $L_R \to \infty$. This makes clear that some other process must halt the cascade and control the mixing length in this limit. In the following sub-section we will argue that, in the absence of a planetary vorticity gradient, the mixing length is ultimately limited by friction.

Before proceeding to the limit case of $\beta = 0$, we shall note that for our simulations with $\beta > 0$ the Rhines scale represents a better approximation for the mixing length than the eddy length scale itself, as diagnosed from the first moment of the EKE spectrum (not shown). This is in qualitative agreement with previous studies, who pointed towards the difference between the mixing and eddy length scales (Thompson and Young, 2007; Ferrari and Nikurashin, 2010; Klocker and Abernathey, 2014).

The f-plane limit

In the f-plane limit ($\beta = 0$), barotropic turbulence theory predicts that quadratic bottom drag halts the inverse EKE cascade when $L = L_f$ (Grianik et al., 2004; Held, 1999). However, as shown in Fig. 6c, L_f over-estimates the dependence of the mixing length on the bottom friction in all simulations, including those with $\beta = 0$. The reason appears to be primarily related to the fact that the bottom flow decouples from the barotropic flow component, thus reducing the impact of changes in the frictional drag.

The frictional arrest scale can be derived by equating the energy flux in the barotropic inverse EKE cascade with the frictional dissipation. The EKE flux in the barotropic cascade may be argued to scale as V_t^3/L_{arr} (e.g. Larichev and Held, 1995), where V_t is the characteristic barotropic eddy velocity and L_{arr} is the arrest scale. Eq. (3) in turn suggests that the frictional dissipation (per unit depth) scales as $C_d V_b^3/H \sim V_b^3/L_f$, where V_b is the eddy velocity in the lower layer. In a purely barotropic flow $V_b = V_t$, and thus $L_{arr} \sim L_f$ (Grianik et al., 2004). For a baroclinic flow, the argument suggests a more general frictional arrest scale

$$[L_{arr}] \equiv ([E_t]/[E_b])^{3/2} L_f. \tag{10}$$

As shown in Fig. 7, this modified arrest scale provides a better estimate for the mixing length than L_f. The dependence of the eddy diffusivity on the bottom drag, however, still appears to be somewhat overestimated. This is likely due to additional losses of EKE, mostly by turbulent advection out of the central jet region, particularly at low friction. This additional energy loss invalidates the assumption of a local balance between the energy cascade rate and the frictional dissipation, which is the basis for the derivation of Eq. (10).

Larichev and Held (1995) proposed to equate the inverse EKE cascade rate with the generation of EKE (rather than the frictional dissipation rate). The generation of EKE is given by Eq. (2), which, with the definition of the Eady growth rate in Eq. (8), suggests a generation rate proportional to $K\sigma_E^2$. If $K \sim LV_t$, a balance between the EKE generation and the cascade rate, V_t^3/L, implies a length scale

$$[L_{LH}] \equiv [E_t]^{1/2}[\sigma]^{-1}. \tag{11}$$

As shown in Fig. 7, Eq. (11) provides a good approximation for the effective mixing length in the limit of $\beta = 0$. For finite β, Eq. (11) generally over-estimates the mixing length (not shown), suggesting that L_{LH} provides another upper bound for L_{mix}.

L_{arr} and L_{LH} are identical if the EKE generation and frictional dissipation balance locally (as will be assumed in Section 4), because both are derived from a balance of the generation/dissipation rate and the scaling for the EKE cascade rate, V_t^3/L. Even though Eq. (11) shows no explicit dependence on the bottom friction, the mixing length is then limited by bottom friction, with the latter entering indirectly in (11), via the dependence on the EKE.

Comparison of L_{LH} with the Rhines scale, L_R, suggests a transition between the f-plane regime and the Rhines scale limited regime when $\beta \sim \sigma^2 E_t^{-1/2}$. Again, a dependence on the bottom friction is implied via the dependence on E_t. We will see in Section 4 that for all our simulations with $\beta > 0$ the Rhines scale remains the limiting factor in controlling the mixing length.

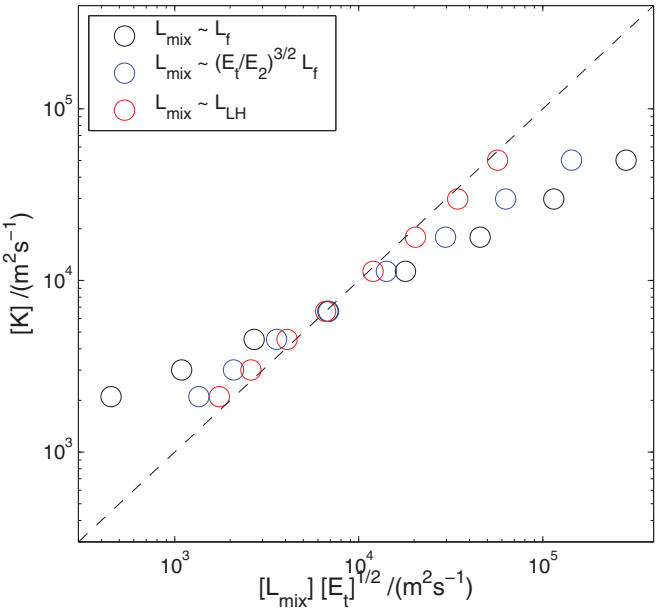

Fig. 7. Bulk eddy diffusivity against estimates based on a mixing length argument: $K_{est} \sim E_t^{1/2} L_{mix}$, for the simulations with $\beta = 0$. Three different choices have been used for the mixing length: $L_{mix} \sim L_f$, $L_{mix} \sim ([E_t]/[E_b])^{3/2} L_f$, and $L_{mix} \sim L_{LH} \equiv [E_t]^{1/2}[\sigma_E]$ – see text for an explanation of the different length scales. For each case the constant factor has been chosen to match the data.

3.5. Bottom flow and barotropic EKE

The EKE budget discussed in Section 2 shows that it is only the EKE near the bottom which enters in the frictional dissipation of mesoscale EKE. The results in Section 3.4 instead show that it is the barotropic component of the eddy velocity which is most important in determining the eddy diffusivity. In this section we discuss what sets the bottom- and barotropic-fraction of the EKE. In general we expect that the inverse energy cascade acts to accumulate energy in the barotropic mode, which then also dominates the bottom flow. Frictional drag, however, will inhibit this barotropization by selectively dissipating EKE in the bottom layer. We will therefore hypothesize that most of the variability in the bottom- and barotropic-fraction of

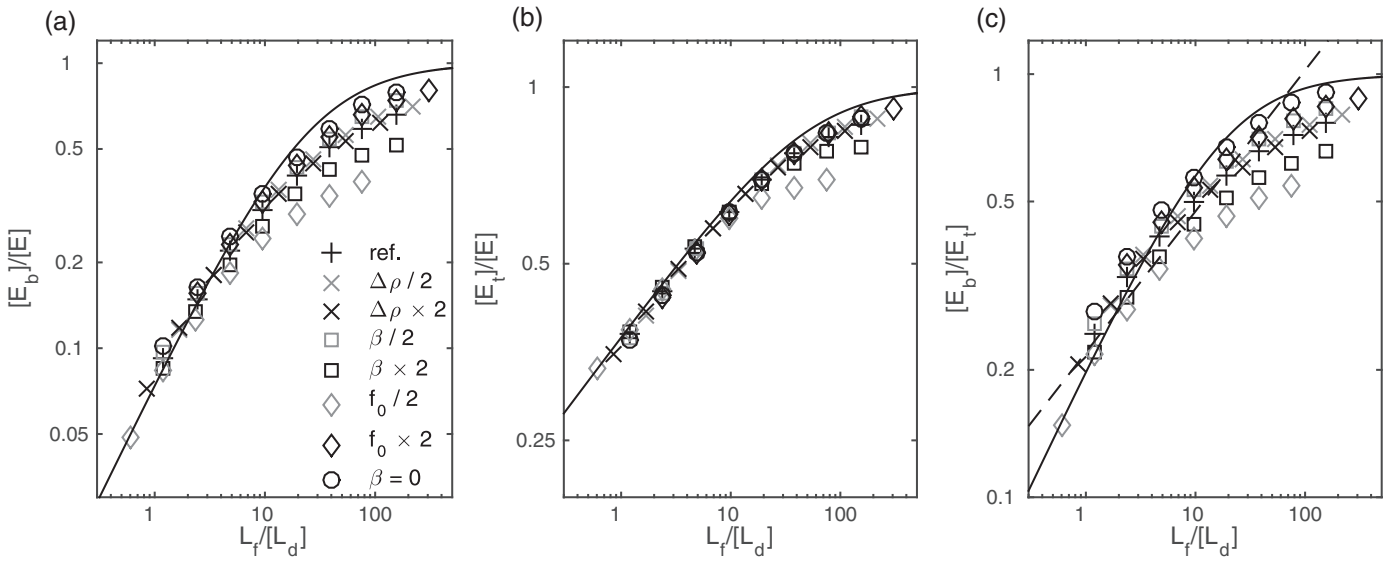

Fig. 8. (a) Ratio of EKE in the bottom layer to vertically averaged EKE, as a function of the frictional parameter L_f/L_d. The solid line shows $[E_b]/[E] = (1 + c_b(L_f/[L_d])^{-1})^{-4/5}$, where $c_b = 25$ was chosen to match the data in the limit of strong friction. (b) Ratio of EKE in the barotropic mode to vertically averaged EKE, as a function of the frictional parameter L_f/L_d. The solid line shows $[E_t]/[E] = (1 + c_t(L_f/[L_d])^{-1})^{-1/4}$, where $c_t = 50$ was again chosen to match the data in the limit of strong friction. (c) Ratio of EKE in the bottom layer to the barotropic mode EKE, as a function of the frictional parameter L_f/L_d. The solid line shows the ratio of the two fits in (a) and (b). The dashed line shows $[E_b]/[E_t] \sim (L_f/[L_d])^{1/3}$. The markers used for the different sets of simulations are as in Fig. 5. Notice the different scales for the y-axis in Figs. (a)–(c).

EKE can be explained by variations in the non-dimensional frictional drag parameter, L_f/L_d.

Fig. 8a shows the ratio of EKE in the bottom layer to the vertically averaged EKE. The ratio varies by over an order of magnitude from less than 0.1 for some of the simulations with the strongest friction (i.e. smallest L_f/L_d) to just under 1 for some of the simulations with the weakest friction (i.e. largest L_f/L_d). The frictional parameter, L_f/L_d, explains most of this variability, though some spread remains, particularly at weak friction. Arbic and Scott (2008) derive scaling relations for homogeneous 2-layer f-plane geostrophic turbulence in the limit of strong quadratic bottom drag. For small L_f/L_d their predictions imply that $E_b/E \sim (L_f/L_d)^{4/5}$. In the limit of large L_f/L_d (i.e. weak drag), we may expect EKE to be dominated by the barotropic mode and thus $E_b/E \to 1$. To mimic this behavior, we propose a functional relation of the form

$$\frac{[E_b]}{[E]} = \left(1 + c_b \frac{[L_d]}{L_f}\right)^{-4/5}, \tag{12}$$

where the constant c_b is chosen to match the simulations in the limit of strong drag. As shown in Fig. 8a, Eq. (12) provides a reasonable fit to the results of the simulations. In the simulations with large β^* (i.e. those with doubled β or halved f_0) the ratio of the bottom layer to total EKE appears to converge to a value smaller than one in the limit of weak friction, so that Eq. (12) more generally provides an upper bound for the bottom fraction of EKE. The weaker bottom signature in the simulations with large β^* is not unexpected, since the planetary vorticity gradient imposes an asymmetry between the layers and acts to inhibit the energy cascade (and thus barotropization). For simplicity we will here not attempt to quantify this additional effect on the vertical structure of the EKE.

Fig. 8 b shows the ratio of the EKE in the barotropic mode to the total (i.e. vertically averaged) EKE. The fraction of EKE in the barotropic mode varies less strongly than the bottom flow fraction over the considered range of simulations, ranging from about 1/3 for the simulation with the smallest L_f/L_d (i.e. strongest drag) to just under 1 in the limit of weak drag. Again, the variability of the barotropic EKE fraction over the considered range of simulations appears to be largely captured by changes in L_f/L_d. For relatively large drag, the fraction of EKE in the barotropic mode appears to scale well with $(L_f/L_d)^{1/4}$. We did not find a satisfactory theoretical explanation for this behavior. Indeed in the limit of very large bottom drag, one may expect the EKE in the bottom layer to become negligible compared to the upper layer EKE (e.g. Arbic and Scott, 2008), in which case one can show that $E_t/E \to h_1/H = 1/4$ for the configuration used here. This limit, however, does not appear to be reached in the present simulations. Based on the empirical power-law scaling found for strong frictional drag, and the expectation that $E_t/E \to 1$ in the limit of weak drag, we propose a functional relation of the form

$$\frac{[E_t]}{[E]} = \left(1 + c_t \frac{[L_d]}{L_f}\right)^{-1/4}, \tag{13}$$

where the constant c_t is again chosen to match the simulations with strong drag. As shown in Fig. 8b, Eq. (13) provides a reasonable fit to the results of the simulations. In the simulations with large β^*, the ratio of barotropic to total EKE again appears to converge to a value somewhat smaller than one in the limit of weak friction – the expected reasons for which are as discussed above.

In Section 4 we will attempt to derive a scaling relation for the eddy diffusivity, assuming a local and instantaneous energy balance. As has been noted by Cessi (2008), the total EKE then drops out, and we only require a scaling relation for the ratio of the EKE near the bottom to the barotropic EKE. Cessi (2008) assumed that this ratio is close to one, arguing that the bottom flow is expected to be dominated by the barotropic mode. The results here, however, suggest that the bottom EKE fraction is more sensitive to changes in the frictional parameter than the barotropic mode EKE fraction. Fig. 8c shows the ratio of EKE in the bottom layer to EKE in the barotropic mode. We find that this ratio varies considerably, ranging from less than 0.2 for the simulation with the smallest L_f/L_d (i.e. strongest drag) to just under one in the limit of weak drag. The explanation for the much stronger decline of the bottom flow (as compared to the barotropic mode) in the limit of large drag may be understood as "baroclinic shielding". The flow in the limit of very strong drag is strongly intensified in the upper ocean. While this upper ocean flow projects significantly onto the barotropic mode, the flow may be vanishingly small near the bottom. The baroclinic mode component in this limit acts to increase the amplitude near the surface while cancelling the amplitude in the deep ocean, thus "shielding" the flow from the

bottom drag. This in-phase coupling between the barotropic and baroclinic modes has been found in observations and ocean state estimates (Müller and Siedler, 1992; Wortham, 2013; Wunsch, 1997).

E_b/E_t is simply the ratio of the quantities shown in Figs. 8a and b, and as a result is reasonably approximated by the ratio of the two fits in Eqs. (8) and (13) (Fig. 8c).

4. The eddy diffusivity from a local EKE balance

The relations derived in Sections 2, 3.4, and 3.5 provide a recipe for the formulation of an eddy parameterization, based on a predictive sub-grid EKE budget equation. The predictive EKE budget-based closure will be discussed in a follow up paper. Here, we instead want to consider the implications of the preceding arguments for the eddy diffusivity assuming a (spatially and temporally) local energy balance.

Under the assumption of a local balance between EKE generation by baroclinic instability and sub-grid EKE dissipation, Eq. (1) becomes

$$\dot{E}_{fric} = \dot{E}_{GM}. \tag{14}$$

From Eq. (2) and the definition of the Eady growth rate (Eq. 8), it can be seen that $\dot{E}_{GM} \sim K\sigma_E^2 \sim E_t^{1/2} L_{mix} \sigma_E^2$. From Eq. (3), and assuming that the bottom flow is dominated by the eddies themselves, one obtains a scaling relation for the frictional dissipation rate as $\dot{E}_{fric} \sim L_f^{-1} E_b^{3/2}$. Eq. (14) thus suggests a scaling relation for the barotropic EKE as

$$E_t \sim \gamma^{-3/2} L_f L_{mix} \sigma_E^2, \tag{15}$$

where we defined $\gamma \equiv E_b/E_t$.

Inserting Eq. (15) into the scaling relation for the eddy diffusivity (Eq. 9) yields

$$K \sim \gamma^{-3/4} L_f^{1/2} L_{mix}^{3/2} \sigma_E. \tag{16}$$

As discussed above, the derivation of a closed scaling relation for the eddy diffusivity, requires arguments for the bottom fraction of EKE, γ, as well as the mixing length, L_{mix}. For easy comparison to previously proposed scaling relations, we are here interested in the derivation of simple power-law relations for the eddy diffusivity, even if they may be valid only over a limited parameter regime. Instead of using the full semi-empirical relation for γ, given by the ratio of Eqs. (8) and (13), we will thus simply approximate $\gamma \sim (L_f/L_d)^{1/3}$, which captures most of the variability of γ outside of the limit of very low bottom friction (Fig. 8c). For the mixing length, we want to consider two different limits: $L_{mix} \sim L_R \sim \beta^{-1/2} E_t^{1/4}$, which in Section 3.4 was found to be appropriate for simulations with non-zero β, and $L_{mix} \sim L_{LH} \sim E_t^{1/2} \sigma_E^{-1}$, which in Section 3.4 was found to be appropriate in the limit where $\beta = 0$. Both scales provide upper bounds for the mixing length.

If we assume $L_{mix} \sim L_R \sim \beta^{-1/2} E_t^{1/4}$ we can use Eqs. (15) and (16) to obtain

$$K \sim \beta^{-1} \gamma^{-3/2} L_f \sigma_E^2 \sim \beta^{-1} L_f^{1/2} L_d^{1/2} \sigma_E^2. \tag{17}$$

Assuming instead that $L_{mix} \sim L_{LH}$ yields

$$K \sim \gamma^{-3} L_f \sigma_E \sim L_f L_d \sigma_E. \tag{18}$$

Eq. (18) could have alternatively been derived using the effective frictional arrest scale from Eq. (10) as the mixing length, i.e. $L_{mix} \sim L_{arr} \sim \gamma^{-3/2} L_f \sim L_f^{1/2} L_d^{1/2}$. As discussed in Section 3.4, L_{arr} and L_{LH} are identical if a local balance is assumed between EKE generation and frictional dissipation. Notice that the frictional arrest scale is found to ultimately depend on both L_f and L_d, because the bottom flow fraction γ is a function of L_f/L_d.

Since both L_R and L_{LH} provide upper bounds for the mixing length, we can more generally define $L_{mix} = \min(L_R, L_{LH})$, which suggests a scaling relation for the eddy diffusivity as

$$K_{est} = \min\left(c_R \beta^{-1} L_f^{1/2} [L_d]^{1/2} [\sigma_E]^2, \quad c_E L_f [L_d][\sigma_E] \right). \tag{19}$$

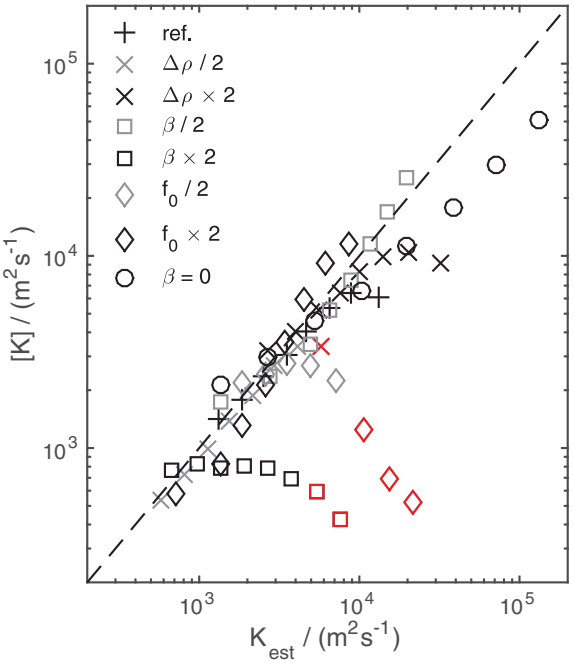

Fig. 9. Eddy diffusivity plotted against the scaling relation in Eq. (19). The markers used for the different sets of simulations are as in Fig. 5. The red markers here denote simulations in which the kinetic energy of the zonal mean flow in the bottom layer exceeds 50% of the EKE (see text). (For interpretation of the references to colour in this figure legend, the reader is referred to the web version of this article.)

Eq. (19) is tested in Fig. 9, with the constants $c_R = 0.06$ and $c_E = 0.7$ chosen such that the respective scaling relations provide overall upper bounds for the observed eddy diffusivity. As already indicated by Fig. 6c, the Rhines scale limits the mixing length in almost all simulations except when $\beta = 0$. The second limiter in Eq. (19) thus becomes important here only for the simulations with $\beta = 0$.

The scaling relation in Eq. (19) provides a reasonable fit to the observed eddy diffusivities over most of the considered simulations. However, Eq. (19) over-estimates the eddy diffusivity in simulations with weak supercriticality and at weak friction. A qualitatively similar behavior was discussed in Section 3.4, where we found that the Rhines scale tends to overestimate the mixing length in these limits. This shortcoming is amplified in the closed scaling relation for the eddy diffusivity, because the over-estimated mixing length also leads to an over-estimate of the EKE. In addition, shortcomings to the energy budget become apparent in this limit. The energy budget in Eq. (14) assumes that all energy is dissipated locally in the form of EKE. In the limit of weak supercriticality and weak friction, however, a significant part of the EKE gets transformed into zonal jets, which do not contribute to meridional mixing, but provide an additional sink for EKE. Since the energy transferred to the mean flow is eventually dissipated by frictional drag acting on the mean KE, the relative influence of this contribution can be measured by considering the ratio of mean flow KE to EKE in the bottom layer. Simulations where the mean KE in the bottom layer exceeds 50% of the EKE are marked in blue in Fig. 9. The results suggest that transfer and eventual dissipation of KE in the mean flow does not appear to be a dominant contributor in most simulations, but does become important in the simulations with the largest misfits. Additional limitations of the local energy budget argument considered here arise from the inhomogeneity of the domain. Specifically, advection of EKE out

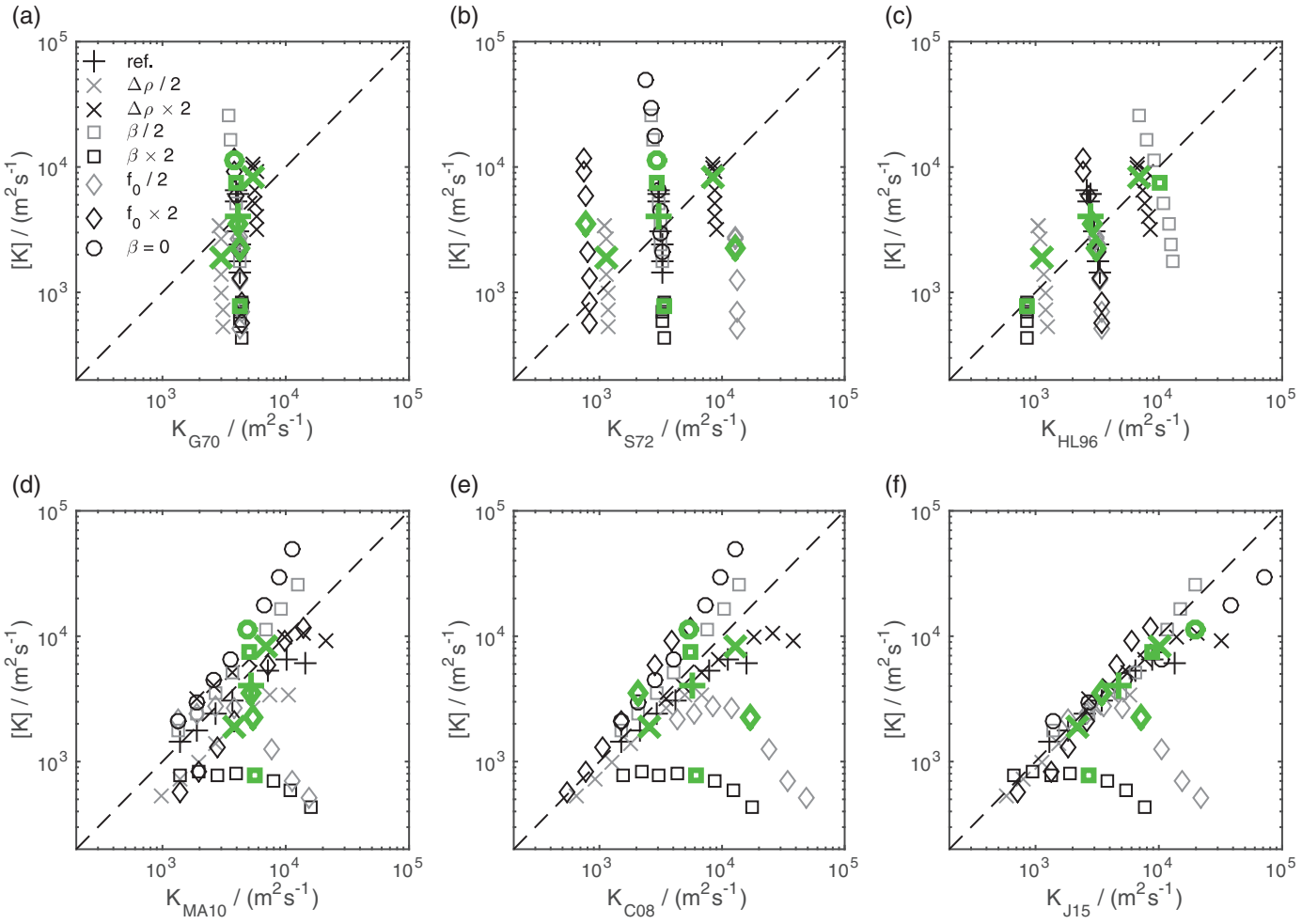

Fig. 10. Comparison of various scaling relations for the eddy diffusivity, tested against the results of the numerical simulations performed for this study. (a) The scaling relation of Green (1970) (Eq. (20)). (b) The scaling relation of Stone (1972) (Eq. (21)). (c) The scaling relation of Held and Larichev (1996) (Eq. (22)). (d) An adaptation of the scaling relation implied in Marshall and Adcroft (2010) for quadratic bottom drag (Eq. (23)). (e) An adaptation of the scaling relation of Cessi (2008) for quadratic bottom drag (Eq. (24)). Panel (f) shows the relation proposed here (Eq. (19)) for easy comparison. The markers used for the different sets of simulations are as in Fig. 5. The bold green markers denote simulations with a fixed drag coefficient, $C_D = 5 \times 10^{-3}$. (For interpretation of the references to colour in this figure legend, the reader is referred to the web version of this article.)

of the central jet region can lead to a significant additional loss of energy.

4.1. Comparison to previous work

In this section we will compare our results to some previously derived relations for the mesoscale eddy diffusivity. The classical scaling arguments proposed by Green (1970), Stone (1972), and Held and Larichev (1996) can all be derived from a balance between the extraction of potential energy from the mean flow (Eq. 2) and the energy flux in the inverse cascade $\sim E_t^{3/2}/L_{mix}$ (Larichev and Held, 1995). The difference between the three formulations arises from different choices for the mixing length - the width of the baroclinic zone in Green (1970), the deformation radius in Stone (1972), and the Rhines scale in Held and Larichev (1996). The resulting scaling relations are

$$K_{G70} = c_{G70} L_{BC}^2 [\sigma_E] \tag{20}$$

$$K_{S72} = c_{S72} [L_d]^2 [\sigma_E] \tag{21}$$

$$K_{HL96} = c_{HL96} \beta^{-2} [\sigma_E]^3 \tag{22}$$

The scaling relation of Green (1970) (Eq. 20) is identical to the approach proposed by Visbeck et al. (1997) which is now commonly used in ocean circulation models (e.g., Farneti and Gent, 2011).

The scaling relations in Eqs. (20)–(22) are tested in Fig. 10a–c. The constant coefficients are chosen to match the data: $c_{G70} = 4 \times 10^{-3}$, $c_{S72} = 4.5$ and $c_{HL96} = 0.15$. By construction, none of the scaling relations predicts a dependence on the bottom friction, which makes them unable to reproduce the dependence of the eddy diffusivity on the frictional drag. The scaling relations of Green (1970) and Stone (1972) are also unable to reproduce changes in the eddy diffusivity associated with other parameter variations. The scaling relation of Held and Larichev (1996) (Eq. (22)) , on the other hand, does capture the bulk of the variation in the eddy diffusivity associated with changes in other external parameters. This is in agreement with the results of Section 3.4, which suggested that the Rhines scale adequately captures the mixing length in most simulations. The results in Fig. 10 emphasize the role of bottom friction, which, for quadratic drag, enters via the frictional length scale, $L_f \sim H/C_D$. The frictional length scale is varied by over two orders of magnitude in our simulations (since we are interested specifically in illuminating the role of bottom friction), while other parameters are varied over at most a factor of four. Over most of the ocean, however, L_f is expected to vary relatively little, so that the scaling relation of Held and Larichev (1996) may perform well for practical purposes.

The mesoscale EKE budget proposed by Eden and Greatbatch (2008) assumes a dissipation rate of EKE independent of bottom drag. Instead the loss of EKE is again assumed to be proportional to the inverse energy cascade rate $E^{3/2}/L_{mix}$. Eden and Greatbatch (2008) then

choose L_{mix} to scale with the deformation radius in mid-and high latitudes, and with the Rhines scale at low latitudes. Assuming a local energy balance, this yields the scaling relation of Stone (1972) (i.e. Eq. (21)) in mid- and high latitudes, and the scaling relation of Held and Larichev (1996) (i.e. Eq. (22)) at low latitudes

The models used in Cessi (2008) and Marshall and Adcroft (2010) applied linear friction, which prevents a direct comparison of their energy budget to our results. However, the fundamental assumptions that go into the derivation of their energy budget-based closure are similar to the ones here, except for the assumptions for the bottom fraction of the EKE, γ, and the mixing length L_{mix}. Both Cessi (2008) and Marshall and Adcroft (2010) choose[4] $\gamma = 1$. Marshall and Adcroft (2010) use a constant mixing length, while Cessi (2008) assumes $L_{mix} = L_d$. Plugging these assumptions into Eq. (16) suggests

$$K_{MA10} = L_c^{3/2} L_f^{1/2} [\sigma_E] \tag{23}$$

$$K_{C08} = c_{C08} [L_d]^{3/2} L_f^{1/2} [\sigma_E] \tag{24}$$

The scaling relations in (23) and (24) are tested against the results of the simulations in Fig. 10d and e, with $L_c = 30$ km and $c_{08} = 1.9$ chosen to match the results of the simulations. Coincidentally, both scaling relations predict the same dependence on the frictional scale, L_f, as found in Eq. (17), which was derived using $\gamma \sim (L_f/L_d)^{1/3}$ and $L_{mix} \sim L_R$. This similarity can be explained by canceling effects: while the use of a constant γ increases the dependence of the eddy diffusivity on the bottom friction, the use of a friction-independent mixing length decreases the sensitivity of the eddy diffusivity on the frictional drag. (The Rhines scale indirectly depends on bottom friction, via its dependence on EKE.) The dependences of both K_{MA} and K_{C08} on other parameters, however, differ from Eq. (17), and generally match the simulations less well. The best overall fit is obtained with the parameterization proposed in this study (Eq. (19)).

The scaling relations in Eqs. (20),(21),(23) and (24), all suggest a linear dependence of the eddy diffusivity on the Eady growth rate, and thus the baroclinicity. This property is a direct consequence of their lack of dependence on β, which here provides the only time-scale in addition to the Eady growth rate. Using the non-dimensionalization discussed in Section 3.3, the eddy diffusivity parameterizations in (20),(21),(23) and (24) are all independent of β^*, or supercriticality. The parameterization of Held and Larichev (1996) (Eq. (22)) implies a quadratic dependence on the supercriticality, and thus a cubic dependence on the baroclinicity, while the parameterization proposed here implies a linear dependence on the supercriticality, and thus a quadratic dependence on the baroclinicity, as long as the mixing length is limited by the Rhines scale (Eq. (19)). Fig. 5b shows that the normalized eddy diffusivity does generally depend on the supercriticality, with the eddy diffusivity increasing for larger supercriticality (i.e. smaller β^*). This dependence is weakest for strong drag and strong supercriticality, and strongest for weak drag and weak supercriticality. As a result, Eq. (22) and Eq. (19) best capture the dependence of the eddy diffusivity on parameters that affect the supercriticality. The parameterization proposed in this paper (Eq. (19)) best captures this dependence for relatively strong drag and/or strong supercriticality, while the parameterization of Held and Larichev (1996) (Eq. (22)) better captures this dependence for relatively weak drag and/or weak supercriticality.

[4] The numerical simulations discussed in Marshall and Adcroft (2010) are barotropic, which makes $\gamma = 1$ the obvious choice. Notice also that the argument in Marshall and Adcroft (2010) differs from the presented approach in that they use a diffusive closure for the PV flux, instead of the interface height or buoyancy flux. Marshall and Adcroft (2010) show that the use of an energy budget-based closure for the eddy PV flux naturally yields some of the stability properties of quasi-geostrophic flows. This is promising and expected to be of importance particularly in the presence of topography, where the implications of PV vs. interface-height diffusion can be quite different.

5. Discussion

Our results imply that over most of the analyzed parameter regime the mixing length is limited by the Rhines scale. However, EKE is dissipated primarily by bottom friction, with only a relatively small part being transferred into eddy-driven jets. To our knowledge such a regime has not been studied systematically in a homogeneous 2D turbulence model. Instead, it is typically assumed that the mixing length is either controlled by bottom friction, in which case β does not enter the scaling for the eddy diffusivity, or by β, in which case bottom friction does not enter scaling arguments for the eddy diffusivity (e.g. Galperin et al., 2010). Smith et al. (2002) derive a scaling relation for the eddy diffusivity in 2D β-plane turbulence with linear drag, under similar assumptions as used here (i.e. a mixing length constrained by the Rhines scale but an eddy energy level limited by bottom friction). However, the simulations discussed in Smith et al. (2002) mostly cover the limit of very weak friction, where a different diffusivity scaling applies. Moreover, we are not aware of any systematic studies of 2D or QG β -plane turbulence in the presence of quadratic bottom drag.

It was argued here that the non-dimensional parameter governing the role of friction is given by the ratio of the frictional length scale, $L_f = H/C_d$, to the deformation radius, L_d. Assuming a drag coefficient $C_d \approx 3 \times 10^{-3}$ (as used in the MOM6 global model), a typical depth of the ocean $H \approx 4\,km$, and deformation radii on the order of $L_d \sim 10$–100 km, suggests $L_f/L_d \sim 10$–100. Somewhat larger frictional drags (corresponding to smaller L_f/L_d) may loosely be justified as a crude representation of the effects of rough bottom topography. These considerations suggest that much of the real ocean is likely in the intermediate drag regime, between the "weak" and "strong" friction limits seen e.g. in Fig. 8. The placement of the ocean in a regime of "intermediate drag", where neither of the typical strong or weak drag limit arguments apply, is also in agreement with the results of Arbic and Flierl (2004).

The scaling relation derived here breaks down for simulations with weakly supercritical mean states and at low frictional drag. In this limit the eddies spin-up strong barotropic jets whose strong shear can suppress eddy mixing via a "barotropic governor" mechanism (James and Gray, 1986). The results of Zurita-Gotor (2007) suggest that this effect may be captured at least partially by including the curvature of the barotopic flow into a generalized definition of the Rhines scale, but this approach was not tested here. The transfer of KE to the mean jets also represents an additional sink of mesoscale EKE. This KE transfer is directly related to the idea of "backscatter" of EKE to the resolved flow (e.g. Jansen and Held, 2014), and could potentially be included in a generalized implementation of the sub-grid EKE budget. The barotropic governor regime is unlikely to be relevant over most of the real ocean, but may be important in localized jets, such as the gulf stream or Kuroshio extension.

It is likely that the Rhines effect, i.e. the transition from turbulence to waves when the Rhines scale is reached, is modified in the real ocean by the presence of topography. Assuming that the barotropic mode remains most relevant for eddy mixing of the ambient baroclinicity, one may argue that the Rhines scale should more generally be replaced by an "effective Rhines scale", where β is modified to include the effect of topographic slopes on the barotropic PV gradient. Such an approach has been used with some success by Grooms et al. (2014). A more detailed investigation into the effects of topography is much-needed.

The ratio of the barotropic EKE to bottom EKE, which was argued to be important in controlling the frictional dissipation of EKE, was found to change primarily with the normalized frictional length scale, L_f/L_d. In a continuously stratified ocean $L_f/L_d \sim C_D^{-1} f/N$. For a constant bottom drag coefficient (as typically assumed in ocean models), our results thus suggest that the bottom fraction of EKE increases with f/N. This qualitative dependence may be expected, as the

ratio f/N is commonly understood to set the aspect ratio of eddies in the ocean. A large Coriolis parameter thus will cause more barotropic eddies, extending to the bottom of the ocean, while strong stratification allows for more surface-intensified eddies with less bottom signature. Ocean observations further appear to point towards stronger barotropization in generally more energetic regions (Wunsch, 1997). This behavior is not expected to be captured adequately by the proposed scaling relation. Instead, such an observation might point towards the necessity to include a dependence of the bottom-flow fraction on the super-criticality. Topography is also likely to be important in governing the vertical structure of the EKE in the real ocean (e.g., Barnier and Le Provost, 1993; Hallberg, 1997). Some effects of rough bottom topography may be expected to broadly resemble those of enhanced bottom drag, but the effect of larger scale topographic features is expected to be qualitatively different from enhanced frictional drag. As with the effect of topography on the mixing length, further investigation into the effects of topography on the vertical structure of eddies is much-needed.

Eddy flux closures that depend on a mesoscale EKE budget naturally rely on an adequate representation of the sink of mesoscale EKE. In the model considered here, kinetic energy is dissipated almost entirely by quadratic bottom friction. Viscous dissipation removes enstrophy, but little energy, due to the lack of a forward energy cascade (see also Jansen and Held, 2014). Unfortunately, the pathways to dissipation of mesoscale EKE in the real ocean are still poorly understood (Ferrari and Wunsch, 2009; Wunsch and Ferrari, 2004). Additional potential pathways to dissipation include the generation of lee waves over rough topography (which eventually break and dissipate their energy - e.g., Nikurashin and Ferrari, 2011), loss of balance in fronts near the surface (which can lead to a forward cascade and eventual dissipation - Molemaker et al., 2010), interactions with internal waves (e.g., Polzin, 2008; Arbic et al., 2013), losses at the western boundaries (e.g., Zhai et al., 2010), and negative wind work (Ferrari and Wunsch, 2009, and references therein). In addition to the shortcomings mentioned before (primarily associated with the role of topography), the pathways of mesoscale EKE to dissipation in the real ocean require further attention. The parameterization proposed here provides a framework which can be extended to include any of these additional processes, once their parametric dependence on the mean flow and EKE field are understood.

6. Summary and conclusions

We discuss the use of a mesoscale eddy kinetic energy budget for the derivation of a scaling relation for the eddy interface height diffusivity or GM coefficient. We show that the success of any energy budget-based parameterization will depend fundamentally on an adequate formulation for the mixing length, as well as an adequate representation of the "bottom signature" of EKE, which is important in determining the amount of frictional dissipation.

For most of the simulations discussed here, the mixing length is very well approximated as proportional to the Rhines scale. This assumption naturally breaks down in the limit of zero β, where instead the energy cascade is arrested by bottom friction. The frictional arrest scale, however, is less sensitive to bottom friction than predicted by barotropic turbulence theory, due to the upper-ocean intensification of EKE.

Eddy mixing is primarily accomplished by the barotropic eddy component, while dissipation is governed by the flow near the bottom, which makes the ratio of the barotropic to bottom EKE important in the formulation of an energy-budget based eddy diffusivity. The ratio of the barotropic EKE to bottom EKE was found to change primarily with the normalized frictional length scale, L_f/L_d. As the effect of bottom drag is increased, eddies tend to become intensified in the upper ocean with weak bottom signatures. In this configuration, the baroclinic part of the flow effectively "shields" the barotropic mode from the effects of bottom friction.

The EKE budget discussed in Section 2, together with the results for the mixing length and bottom fraction of EKE from Sections 3.4 and 3.5, provides a general recipe that can be used to formulate an eddy closure based on a prognostic sub-grid mesoscale EKE budget. A local prognostic EKE budget, based on these results, is currently being implemented in GFDL's ocean model, and is expected to be the topic of a follow-up paper. Here we instead estimate the EKE budget-based eddy diffusivity, assuming a temporally and spatially local EKE balance. The resulting scaling relation (Eq. (19)) provides an adequate fit for most of our simulations. Eq. (19) outperformed various scaling relations that have been proposed previously, including the one proposed by Green (1970) and Visbeck et al. (1997), which is commonly used in ocean models. The scaling relation of Held and Larichev (1996) adequately captures the dependence of the eddy diffusivity on various mean flow parameters, while it is by construction unable to represent the dependence on the bottom friction.

The general results found here are in agreement with those found in quasi-geostrophic models (e.g. Larichev and Held, 1995; Held and Larichev, 1996; Pavan and Held, 1996; Lapeyre and Held, 2003; Thompson and Young, 2007). Further study of the dependence of eddy fluxes on frictional dissipation within a QG framework is thus expected to provide valuable insights. Since any such model depends on the parameterization of frictional dissipation, we further need to better understand the pathways to dissipation in the ocean. Progress on this question can likely be made using a combination of observations and high-resolution models, which can explicitly resolve the processes that lead to loss of balance and eventual dissipation.

Acknowledgments

We would like to thank Stephen Griffies, Adele Morrison, David Marshall and an anonymous reviewer for their valuable comments, which helped to improve of the manuscript. M.F.J. acknowledges funding from a NOAA Climate and Global Change Postdoctoral Fellowship, administered by the University Corporation for Atmospheric Research. A.J.A. was supported under awards NA08OAR4320752 and NA14OAR4320106 from the National Oceanic and Atmospheric Administration, U.S. Department of Commerce. The statements, findings, conclusions, and recommendations are those of the authors and do not necessarily reflect the views of the National Oceanic and Atmospheric Administration, or the U.S. Department of Commerce.

References

Abernathey, R., Ferreira, D., Klocker, A., 2013. Diagnostics of isopycnal mixing in a circumpolar channel. Ocean Modell. 72, 1–16.
Abernathey, R.P., Marshall, J., 2013. Global surface eddy diffusivities derived from satellite altimetry. J. Geophys. Res.: Oceans 118.2, 901–916.
Arbic, B.K., Flierl, G.R., 2004. Baroclinically unstable geostrophic turbulence in the limits of strong and weak bottom ekman friction: application to midocean eddies. J. Phys. Oceanogr. 34, 2257–2273.
Arbic, B.K., Polzin, K.L., Scott, R.B., Richman, J.G., Shriver, J.F., 2013. On eddy viscosity, energy cascades, and the horizontal resolution of gridded satellite altimeter products. J. Phys. Oceanogr. 43, 283–300.
Arbic, B.K., Scott, R.B., 2008. On quadratic bottom drag, geostrophic turbulence, and oceanic mesoscale eddies. J. Phys. Oceanogr. 38, 84–103.
Barnier, B., Le Provost, C., 1993. Influence of bottom topography roughness on the jet and inertial recirculation of a mid-latitude gyre. Dyn. Atm. Oceans 18, 29–65.
Cessi, P., 2008. An energy-constrained parameterization of eddy buoyancy flux. J. Phys. Oceanogr. 38, 1807–1819.
Chelton, D.B., Schlax, M.G., Samelson, R.M., de Szoeke, R.A., 2007. Global observations of large oceanic eddies. Geophys. Res. Lett. 34, L15 606.
Early, J.J., Samelson, R.M., Chelton, D.B., 2011. The evolution and propagation of quasi-geostrophic ocean eddies. J. Phys. Oceanogr. 41 (8), 1535–1555.
Eden, C., Greatbatch, R.J., 2008. Towards a mesoscale eddy closure. Ocean Modell. 20 (3), 223–239.
Egbert, G.D., Ray, R.D., Bills, B.G., 2004. Numerical modeling of the global semidiurnal tide in the present day and in the last glacial maximum. J. Geophys. Res.: Oceans 109 (C3).

Farneti, R., Gent, P.R., 2011. The effects of the eddy-induced advection coefficient in a coarse-resolution coupled climate model. Ocean Modell. 39 (1–2), 135–145 Modelling and Understanding the Ocean Mesoscale and Submesoscale.
Ferrari, R., Nikurashin, M., 2010. Suppression of eddy mixing across jets in the southern ocean. J. Phys. Oceanogr. 40, 1501–1519.
Ferrari, R., Wunsch, C., 2009. Ocean circulation kinetic energy–reservoirs, sources and sinks. Ann. Rev. Fluid Mech. 41, 253–282.
Flato, G., Marotzke, J., Abiodun, B., Braconnot, P., Chou, S., Collins, W., Cox, P., Driouech, F., Emori, S., Eyring, V., Forest, C., Gleckler, P., Guilyardi, E., Jakob, C., Kattsov, V., Reason, C., Rummukainen, M., 2013. Evaluation of climate models. In: Stocker, T., Qin, D., Plattner, G.-K., Tignor, M., Allen, S., Boschung, J., Nauels, A., Xia, Y., Bex, V., Midgley, P. (Eds.), In: Climate Change 2013: The Physical Science Basis. Contribution of Working Group I to the Fifth Assessment Report of the Intergovernmental Panel on Climate Change. Cambridge University Press, Cambridge, United Kingdom and New York, NY, USA.
Flierl, G.R., 1978. Models of vertical structure and the calibration of two-layer models. Dyn. Atm. Oceans 2, 341–381.
Galperin, B., Sukoriansky, S., Dikovskaya, N., 2010. Geophysical flows with anisotropic turbulence and dispersive waves: flows with a β-effect. Ocean Dyn. 60 (2), 427–441.
Gent, P.R., McWilliams, J.C., 1990. Isopycnal mixing in ocean circulation models. J. Phys. Oceanogr. 20, 150–155.
Gent, P.R., Willebrand, J., McDougall, T.J., McWilliams, J.C., 1995. Parameterizing eddy-induced tracer transports in ocean circulation models. J. Phys. Oceanogr. 25, 463–474.
Gill, A.E., 1982, vol. 30. Atmosphere–Ocean Dynamics. Academic Press.
Gill, A.E., Green, J.S.A., Simmons, A.J., 1974. Energy partition in the large-scale ocean circulation and the production of mid-ocean eddies. Deep Sea Res. 21 (7), 499–528.
Green, J.S.A., 1970. Transfer properties of the large-scale eddies and the general circulation of the atmosphere. Quart. J. Roy. Meteor. Soc. 96, 157–185.
Grianik, N., Held, I.M., Smith, K.S., Vallis, G.K., 2004. The effects of quadratic drag on the inverse cascade of two-dimensional turbulence. Phys. Fluids 16 (1), 73–78.
Griffies, S.M., Halberg, R., 2000. Biharmonic friction with a Smagorinsky-like viscosity for use in large-scale eddy-permitting ocean models. Mon. Wea. Rev. 128, 2935–2946.
Grooms, I., Majda, A.J., Smith, K.S., 2014. Stochastic superparameterization in a quasi-geostrophic model of the antarctic circumpolar current. Ocean Model. Accepted.
Hallberg, R., 1997. Localized coupling between surface and bottom-intensified flow over topography. J. Phys. Oceanogr. 27, 977–998.
Hallberg, R., 2013. Using a resolution function to regulate parameterizations of oceanic mesoscale eddy effects. Ocean Modell. 72, 92–103.
Hallberg, R., Gnanadesikan, A., 2006. The role of eddies in determining the structure and response of the wind-driven southern hemisphere overturning: results from the Modeling Eddies in the Southern Ocean (MESO) project. J. Phys. Oceanogr. 36 (12), 2232–2252.
Held, I.M., 1999. The macroturbulence of the troposphere. Tellus 51, 59–70.
Held, I.M., Larichev, V.D., 1996. A scaling theory for horizontally homogeneous baroclinically unstable flow on a beta plane. J. Atmos. Sci. 53 (7), 946–952.
James, I.N., Gray, L.J., 1986. Concerning the effect of surface drag on the circulation of a baroclinic planetary atmosphere. Quart. J. Roy. Meteor. Soc. 1112, 1231–1250.
Jansen, M., Ferrari, R., 2013. Equilibration of an atmosphere by adiabatic eddy fluxes. J. Atmos. Sci. 70, 2948–2962.
Jansen, M.F., Held, I.M., 2014. Parameterizing subgrid-scale eddy effects using energetically consistent backscatter. Ocean Modell. 80, 36–48.
Johnson, G.C., Bryden, H.L., 1989. On the size of the antarctic circumpolar current. Deep Sea Res. Part A. Oceanogr. Res. Pap. 36 (1), 39–53.
Klocker, A., Abernathey, R., 2014. Global patterns of mesoscale eddy properties and diffusivities. J. Phys. Oceanogr. 44, 1030–1046.
Klocker, A., Marshall, D.P., 2014. Advection of baroclinic eddies by depth mean flow. Geophys. Res. Lett. 41 (10), 3517–3521.
Lapeyre, G., Held, I.M., 2003. Diffusivity, kinetic energy dissipation, and closure theories for the poleward eddy heat flux. J. Atmos. Sci. 60 (23), 2907–2916.
Larichev, V.D., Held, I.M., 1995. Eddy amplitudes and fluxes in a homogeneous model of fully developed baroclinic instability. J. Phys. Oceanogr. 25, 2285–2297.
Ledwell, J.R., Montgomery, E.T., Polzin, K.L., St. Laurent, L.C., Schmitt, R.W., Toole, J.M., 2000. Evidence for enhanced mixing over rough topography in the abyssal ocean. Nature 403 (6766), 179–182.
Marshall, D.P., Adcroft, A.J., 2010. Parameterization of ocean eddies: potential vorticity mixing, energetics and Arnold's first stability theorem. Ocean Modell. 32 (3–4), 188–204 The magic of modelling: a special volume commemorating the contributions of Peter D. Killworth–Part 2.
Mazloff, M., Ferrari, R., Schneider, T., 2013. The force balance of the southern ocean meridional overturning circulation. J. Phys. Oceanogr. 43 (6), 1193–1208.
McWilliams, J.C., 2008. The nature and consequences of oceanic eddies. In: Geophysical Monograph Series, vol. 177. American Geophysical Union, Washington, D.C., pp. 5–15.
Molemaker, M.J., MCWilliams, J.C., Capet, X., 2010. Balanced and unbalanced routes to dissipation in an equilibrated eady flow. J. Fluid Mech. 654, 35–63.
Müller, T.J., Siedler, G., 1992. Multi-year current time series in the eastern north atlantic ocean. J. Mar. Res. 50, 63–98.
Nakamura, N., Wang, L., 2013. On the thickness ratio in the quasigeostrophic two-layer model of baroclinic instability. J. Atmos. Sci. 70 (5), 1505–1511.
Nikurashin, M., Ferrari, R., 2011. Global conversion rate from geostrophic flows into internal lee waves in the deep ocean. Geophys. Res. Lett. 38, L08610.
Nikurashin, M., Vallis, G., Adcroft, A., 2013. Routes to energy dissipation for geostrophic flows in the southern ocean. Nat. Geosci. 6, 48–51.
Özgökmen, T.M., Fischer, P.F., 2008. On the role of bottom roughness in overflows. Ocean Modell. 20 (4), 336–361.
Pavan, V., Held, I., 1996. The diffusive approximation for eddy fluxes in baroclinically unstable jets. J. Atmos. Sci. 53 (9), 1262–1272.
Plumb, R., 1979. Eddy fluxes of conserved quantities by small-amplitude waves. J. Atmos. Sci. 36 (9), 1699–1704.
Polzin, K.L., 2008. Mesoscale eddyinternal wave coupling. Part I: symmetry, wave capture, and results from the mid-ocean dynamics experiment. J. Phys. Oceanogr. 38, 2556–2574.
Prandtl, L., 1925. Bericht über untersuchungen zur ausgebildeten turbulenz. Zeitschr. angew. Math. Mech. 5, 136–139.
Redi, M., 1982. Oceanic isopycnal mixing by coordinate rotation. J. Phys. Oceanogr. 12, 1154–1158.
Rhines, P.B., 1979. Geostrophic turbulence. Annu. Rev. Fluid Mech. 11, 401–441.
Smagorinsky, J., 1963. General circulation experiments with the primitive equations. Mon. Wea. Rev. 91, 99–164.
Smith, K.S., Boccaletti, G., Henning, C.C., Marinov, I.N., Tam, C.Y., Held, I.M., Vallis, G.K., 2002. Turbulent diffusion in the geostrophic inverse cascade. J. Fluid Mech. 469, 13–48.
Stone, P.H., 1972. A simplified radiative-dynamical model for the static stability of rotating atmospheres. J. Atmos. Sci. 29 (3), 405–418.
Thompson, A., Young, W., 2007. Two-layer baroclinic eddy heat fluxes: zonal flows and energy balance. J. Atmos. Sci. 64, 3214–3231.
Vallis, G., 1988. A numerical study of transport properties in eddy resolving and parameterized models. Quart. J. Roy. Meteor. Soc. 114, 183–204.
Vallis, G.K., 2006. Atmospheric and Oceanic Fluid Dynamics. Cambridge University Press, Cambridge, U.K..
Visbeck, M., Marshall, J., Haine, T., Spall, M., 1997. Specification of eddy transfer coefficients in coarse-resolution ocean circulation models. J. Phys. Oceanogr. 27, 381–402.
Waterman, S., Hogg, N.G., Jayne, S.R., 2011. Eddy-mean flow interaction in the Kuroshio extension region. J. Phys. Oceanogr. 41, 1182–1208.
Willebrand, J., Barnier, B., Böning, C., Dieterich, C., Killworth, P.D., Provost, C.L., Jia, Y., Molines, J.-M., New, A.L., 2001. Circulation characteristics in three eddy-permitting models of the north atlantic. Prog. Oceanogr. 48 (23), 123–161 Dynamics of the North Atlantic Circulation: Simulation and Assimilation with High-Resolution Models (DYNAMO).
Wortham, C., 2013. A multi-dimensional spectral description of ocean variability with applications. MIT/WHOI Joint Program Ph.D. thesis.
Wunsch, C., 1997. The vertical partition of oceanic horizontal kinetic energy. J. Phys. Oceanogr. 27, 1770–1794.
Wunsch, C., Ferrari, R., 2004. Vertical mixing, energy, and the general circulation of the oceans. Annu. Rev. Fluid Mech. 36, 281–314.
Zhai, X., Johnson, H.L., Marshall, D.P., 2010. Significant sink of ocean-eddy energy near western boundaries. Nat. Geosci. 3 (9), 608–612.
Zurita-Gotor, P., 2007. The relation between baroclinic adjustment and turbulent diffusion in the two-layer model. J. Atmos. Sci. 64, 1284–1300.